The Astrophysical Journal, 836:140 (12pp), 2017 February 10 doi:10.3847/1538-4357/836/1/140

A Hard Look at the Neutron Stars and Accretion Disks in 4U 1636-53, GX 17+2, and 4U 1705-44 with *NuStar*

R. M. Ludlam[1], J. M. Miller[1], M. Bachetti[2], D. Barret[3,4], A. C. Bostrom[1], E. M. Cackett[5], N. Degenaar[6,7], T. Di Salvo[8], L. Natalucci[9], J. A. Tomsick[10], F. Paerels[11], and M. L. Parker[6]
[1] Department of Astronomy, University of Michigan, 1085 South University Avenue, Ann Arbor, MI 48109-1107, USA
[2] INAF/Osservatorio Astronomico di Cagliari, via della Scienza 5, I-09047 Selargius (CA), Italy
[3] Université de Toulouse; UPS-OMP; IRAP; Toulouse, France
[4] CNRS; Institut de Recherche en Astrophysique et Plantologie; 9 Av. colonel Roche, BP 44346, F-31028 Toulouse cedex 4, France
[5] Department of Physics & Astronomy, Wayne State University, 666 W. Hancock Street, Detroit, MI 48201, USA
[6] Institute of Astronomy, Madingley Road, Cambridge CB3 0HA, UK
[7] Anton Pannekoek Institute for Astronomy, University of Amsterdam, Pastbus 94249, 1090 GE Amsterdam, The Netherlands
[8] Dipartimento di Fisica e Chimica, Universitá degli Studi di Palermo, via Archirafi 36, I-90123, Palermo, Italy
[9] Istituto Nazionale di Astrofisica, INAF-IAPS, via del Fosso del Cavaliere, I-00133 Roma, Italy
[10] Space Sciences Laboratory, 7 Gauss Way, University of California, Berkeley, CA 94720-7450, USA
[11] Columbia Astrophysics Laboratory, 550 West 120th Street, New York, NY 10027, USA
Received 2016 August 5; revised 2017 January 4; accepted 2017 January 6; published 2017 February 14

Abstract

We present *NuSTAR* observations of neutron star (NS) low-mass X-ray binaries: 4U 1636-53, GX 17+2, and 4U 1705-44. We observed 4U 1636-53 in the hard state, with an Eddington fraction, $F_{\rm Edd}$, of 0.01; GX 17+2 and 4U 1705-44 were in the soft state with fractions of 0.57 and 0.10, respectively. Each spectrum shows evidence for a relativistically broadened Fe K_α line. Through accretion disk reflection modeling, we constrain the radius of the inner disk in 4U 1636-53 to be $R_{\rm in} = 1.03 \pm 0.03$ ISCO (innermost stable circular orbit), assuming a dimensionless spin parameter $a_* = cJ/GM^2 = 0.0$, and $R_{\rm in} = 1.08 \pm 0.06$ ISCO for $a_* = 0.3$ (errors quoted at 1σ). This value proves to be model independent. For $a_* = 0.3$ and $M = 1.4\ M_\odot$, for example, 1.08 ± 0.06 ISCO translates to a physical radius of $R = 10.8 \pm 0.6$ km, and the NS would have to be smaller than this radius (other outcomes are possible for allowed spin parameters and masses). For GX 17+2, $R_{\rm in} = 1.00$–1.04 ISCO for $a_* = 0.0$ and $R_{\rm in} = 1.03$–1.30 ISCO for $a_* = 0.3$. For $a_* = 0.3$ and $M = 1.4\ M_\odot$, $R_{\rm in} = 1.03$–1.30 ISCO translates to $R = 10.3$–13.0 km. The inner accretion disk in 4U 1705-44 may be truncated just above the stellar surface, perhaps by a boundary layer or magnetosphere; reflection models give a radius of 1.46–1.64 ISCO for $a_* = 0.0$ and 1.69–1.93 ISCO for $a_* = 0.3$. We discuss the implications our results may have on the equation of state of ultradense, cold matter and our understanding of the innermost accretion flow onto NSs with low surface magnetic fields, and systematic errors related to the reflection models and spacetime metric around less idealized NSs.

Key words: accretion, accretion disks – stars: neutron – X-rays: binaries – X-rays: individual (4U 1636-53, GX 17 +2, 4U 1705-44)

1. Introduction

The equation of state (EOS) of ultradense matter is not yet known. Earth laboratories are unable to replicate the necessary environment to constrain the EOS. Thus, the only way to study matter under these extreme conditions is through observations of neutron stars (NSs). The EOS sets the mass and radius of the NS. Theoretical mass–radius tracks have been compiled for different theoretical models (see Lattimer & Prakash 2016 for a review). Three-body interactions between nucleons make the radius of the NS the most important quantity in determining the EOS because it does not change quickly as a function of mass. Hence, constraining the radius of the NS can, in turn, lead to a determination of the EOS of the cold, dense matter under extremely dense physical conditions (Lattimer 2011).

Low-mass X-ray binaries (LMXBs) are one setting in which we can attempt to constrain the EOS through observations. LMXBs consist of a roughly stellar-mass companion that transfers matter onto a compact object via Roche-lobe overflow. Broad iron line profiles have been seen in these accreting systems that harbor a black hole (BH; e.g., Fabian et al. 1989; Miller et al. 2002; Miller 2007; Reis et al. 2008, 2009a) or NS (e.g., Bhattacharyya & Strohmayer 2007; Cackett et al. 2008, 2009, 2010; Papitto et al. 2008; di Salvo et al. 2009; Egron et al. 2013; Miller et al. 2013; Di Salvo et al. 2015) as the primary accreting compact object. LMXBs are ideal laboratories for conducting radius measurements through reflection studies since all accretion occurs via the disk, as opposed to their high-mass X-ray binary (HMXB) counterparts, which can accrete via stellar winds.

X-ray disk lines are produced from an external hard X-ray source irradiating the accretion disk. In the case of NSs, the hard X-ray source could be a hot corona, the stellar surface, or a boundary layer and may be thermal or nonthermal in nature. Regardless of the nature of the hard X-ray emission, the asymmetrically broadened profile of the Fe K_α line gives a direct measure of the position of the inner disk since the effects of gravitational redshift and Doppler redshift/boosting on the emission line become stronger closer to the compact object (Fabian et al. 1989).

The Fe K_α line in NS LMXBs can set an upper limit for the radius of NSs since the disk must truncate at or before the surface (Cackett et al. 2008, 2010; Reis et al. 2009b; Miller et al. 2013; Degenaar et al. 2015). Since the magnetic field could also truncate the accretion disk, studies of disk reflection

can also be used to set an upper limit on the magnetic field strength (Cackett et al. 2009; Papitto et al. 2009; Miller et al. 2011; Degenaar et al. 2014, 2016; King et al. 2016; Ludlam et al. 2016).

We analyze *NuSTAR* (Harrison et al. 2013) observations of NS LMXBs 4U 1636-53, GX 17+2, and 4U 1705-44. 4U 1636-53 and 4U 1705-44 are categorized as atoll sources while GX 17+2 is a "Z" source, according to the classification of Hasinger & van der Klis (1989). Atoll sources have lower luminosities ($\sim$0.01–0.2 $L_{\rm Edd}$) than Z sources (see Done et al. 2007 for a review). Z sources have soft X-ray spectra that can be described by two thermal components (multicolor disk blackbody and single-temperature blackbody; Lin et al. 2007). Atolls can have soft or hard spectra with transitional phases in between. The hard state can be modeled well by a power law and thermal component when needed (Lin et al. 2007).

Further, the spectral state may be associated with the level of disk truncation (Done et al. 2007). A study of 4U 1608-52 by Gierliński & Done (2002) found that at low luminosity, the accretion disk was truncated, while at high luminosity, the inner radius of the disk moved inwards. Pintore et al. (2016) found a similar behavior for SAX J1748.9-2021. However, Sanna et al. (2014) found that the inner disk did not seem to be correlated with the spectral state for 4U 1636-53. The inner disk radius of Serpens X-1 (Ser X-1) also does not appear to change much for a range of luminosities (Chiang et al. 2016).

4U 1636-53 was in the hard state at the time of the *NuSTAR* observation, while GX 17+2 and 4U 1705-44 were in the soft state. We focus on constraining the inner disk radius in these sources and the implications this has on the EOS for ultradense, cold matter. The following sections (Sections 1.1–1.3) give a brief introduction to each source. Section 2 provides details on the observations of each source and how the data were reduced. Section 3 presents our analysis and results. Section 4 discusses those results, and we conclude in Section 5.

1.1. 4U 1636-53

4U 1636-53 is a well-studied, persistent LMXB that exhibits type 1 X-ray bursts and has a tentative spin frequency of 581 Hz (Zhang et al. 1997; Strohmayer & Markwardt 2002). The source is located a maximum of 6.6 kpc away from inspection of the type 1 X-ray bursts (assuming the brightest type 1 X-ray bursts hit the Eddington limit; Galloway et al. 2008). The companion star is a 0.4 $M_{\odot}$, 18th magnitude star with an orbital period of 3.8 hr (Pedersen et al. 1982; van Paradijs et al. 1990). Kilohertz quasi-periodic oscillations (QPOs) suggest that 4U 1636-53 may harbor an NS as large as 2 $M_{\odot}$ (Barret et al. 2006; Casares et al. 2006). The system regularly undergoes state transitions on $\sim$40 day time intervals (Shih et al. 2005).

Reflection studies suggest this source has a high inclination, but a lack of dips in the X-ray light curve limits the inclination $\sim$70° (Frank et al. 1987; Casares et al. 2006; Sanna et al. 2013). Pandel et al. (2008) found that the inner disk radius was consistent with the innermost stable circular orbit (ISCO) when looking at observations taken with *XMM-Newton* and *RXTE* while in the transitional and soft state. Cackett et al. (2010) found larger inner disk radii at $\sim 8 \pm 4$ ISCO (assuming $a_* = 0$) when applying blurred reflection models to the low flux state, but values consistent with the ISCO were measured in the soft state. Additionally, Sanna et al. (2013) analyzed the source in the soft and transitional states with two additional observations. They measure the inner disk radius to be as large as 4.45 ISCO in low flux states, which is smaller but consistent with Cackett et al. (2010). Lyu et al. (2014) used observations from *Suzaku*, *XMM-Newton*, and *RXTE* to see if the inner disk radius inferred from the Fe line changed over flux states. They used available disk line models (DISKLINE, LAOR, KRYLINE) to account for relativistic broadening and found that the Fe line did not change significantly. They conclude that the line is broadened by mechanisms other than just relativistic broadening, although the data are consistent with a disk remaining at the ISCO if timing parameters trace the mass accretion rate rather than the inner radius.

1.2. GX 17+2

GX 17+2 is a burster located a maximum distance of 13.0 kpc (Galloway et al. 2008) with a tentative spin frequency of 293.2 Hz (Wijnands et al. 1997). The counterpart of GX 17+2 is not known currently. It may be NP Ser (Tarenghi & Reina 1972) or star "A" proposed by Deutsch et al. (1999) from optical and IR variability studies. However, Callanan et al. (2002) proposed that the IR variability could be explained by synchrotron flares. The system has an inclination of less than 45° (Cackett et al. 2010, 2012). Di Salvo et al. (2000) performed the first extensive spectral analysis of GX 17+2. They were able to limit the radius of the NS between 10–19 km based upon Comptonization of photons within their spectra. Cackett et al. (2010) found a similarly small limit through modeling the Fe reflection in the accretion disk.

1.3. 4U 1705-44

4U 1705-44 is a persistently bright source that shows type 1 X-ray bursts (Langmeier et al. 1987) which place it at a maximum distance of 7.8 kpc (Galloway et al. 2008). The source has been observed in both the hard and soft states (Barret & Olive 2002; Piraino et al. 2007). Broad Fe emission has been observed in each of these states. The inclination of the system is between 20° and 50° (Piraino et al. 2007). di Salvo et al. (2009) found evidence for multiple emission lines for S XVI, Ar XVIII, and Ca XIX in addition to iron in observations taken with *XMM-Newton*. These lines gave an inner disk radius of 2.3 ± 0.3 ISCO (assuming $a_* = 0$). Reis et al. (2009b) found an inner disk radius of $1.75^{+0.17}_{-0.28}$ ISCO when using observations obtained with *Suzaku*. Cackett et al. (2010) used both *XMM-Newton* and *Suzaku* observations and found that the inner disk ranged from 1.0 to 6.5 ISCO. The inner disk of 4U 1705-44 appears to be truncated in many studies although the degree of truncation varies.

2. Observations and Data Reduction

The details of each *NuSTAR* observation are listed in Table 1. Light curves and spectra were created using a 120″ circular extraction region centered around the source using the NUPRODUCTS tool from NUSTARDAS v1.5.1 with CALDB 20160421. A background was generated and subtracted using another region of the same dimension in a region away from the source. There were a total of six type 1 X-ray bursts present in the light curves for 4U 1636-53 and a single type 1 X-ray burst for 4U 1705-44. We will report on the bursts in a separate paper. We created good time intervals (GTIs) to remove $\sim$10–150 s after the initial fast rise (depending on the duration of the individual burst) to separate these from the steady emission. These GTIs were applied during the generation of the

Table 1
NuSTAR Observation Information

Source	Obs ID	Date	Net Exp (ks)	Net Rate (cts s^{-1})
4U 1636-53	30101024002	2015 Jun 06	19.2	40
GX 17+2	30101023002	2016 Mar 22	23.3	361
4U 1705-44	30101025002	2016 Apr 22	28.7	174

spectra for both the FPMA and FPMB. Initial modeling of the persistent emission spectra with a constant, fixed to 1 for the FPMA and allowed to float for the FPMB, found the floating constant to be within 0.95–1.05 in each case. We proceeded to combine the two source spectra, background spectra, and ancillary response matrices via ADDASCASPEC. We use ADDRMF to create a single redistribution matrix file. The spectra were grouped using GRPPHA to have a minimum of 25 counts per bin (Cash 1979).

3. Spectral Analysis and Results

We use XSPEC version 12.8.1 (Arnaud et al. 1996) in this work. All errors are quoted at the 1σ (68%) confidence level and were calculated from Monte Carlo Markov Chain (MCMC) of length 100,000. We perform fits over the energy range in which the spectrum is not background dominated for each source. We account for the neutral column hydrogen density along the line of sight via TBABS (Wilms et al. 2000). The solar abundance was set to WILM (Wilms et al. 2000) and VERN cross-sections (Verner et al. 1996) were used.

We experimented with different phenomenological one-, two-, and three-component models to describe the spectral continua. None of the sources required three components. The continuum of the spectrum obtained from 4U 1636−53 was well-described with a cut-off power-law model. The cut-off energy may reflect the electron temperature of the corona, and the simple continuum component may only be an approximation of a region dominated by Comptonization. The spectral continua of GX 17+2 and 4U 1705−44 were well-described by a combination of disk blackbody (Mitsuda et al. 1984) and simple blackbody components. It is possible to infer radii from both disk blackbody and simple blackbody components; however, it is also clear that scattering can harden emergent spectra and cause falsely small radii to be inferred (e.g., London et al. 1986; Shimura & Takahara 1995; Merloni et al. 2000). Low temperature, optically-thick Comptonization can sometimes be approximated as a blackbody; it is likely that our simple blackbody component accounts for this process in the boundary layer (e.g., Gilfanov et al. 2003). Given the many complexities and possible distortions, we do not look to the continua for robust physical inferences; rather, we utilize disk reflection for this purpose.

To properly describe the reflection features and relativistic effects present in the data for 4U 1636-53, we employ the model RELXILL (García et al. 2014). This model self-consistently accounts for X-ray reflection and relativistic ray tracing for a power law irradiating an accretion disk while properly taking into account the inclination in the reflection from the disk. The parameters of this model are as follows: inner emissivity ($q_{\rm in}$), outer emissivity ($q_{\rm out}$), break radius ($R_{\rm break}$) between the two emissivities, spin parameter ($a_* = cJ/GM^2$), inclination of the disk (i), inner radius of the disk ($R_{\rm in}$) in units of ISCO, outer radius of the disk ($R_{\rm out}$), redshift (z), photon index of the power law(Γ), log of the ionization parameter ($\log(\xi)$), iron abundance ($A_{\rm Fe}$), cut-off energy of the power law ($E_{\rm cut}$), reflection fraction ($f_{\rm refl}$), and normalization.

We apply BBREFL (Ballantyne 2004) to GX 17+2 and 4U 1705-44 in order to model the emergent reflection emission from a disk assuming an irradiating blackbody continuum, and convolve it with RELCONV (Dauser et al. 2010). The iron abundance in BBREFL comes in two flavors: solar abundance and twice the solar abundance. The parameters of BBREFL are as follows: log of the ionization parameter ($\log(\xi)$), temperature of the incident blackbody in keV (kT), iron abundance ($A_{\rm Fe}$), reflection fraction ($f_{\rm refl}$), redshift (z), and normalization. The parameters of RELCONV are as follows: inner emissivity index ($q_{\rm in}$), outer emissivity index ($q_{\rm out}$), dimensionless spin parameter (a_*), inner disk radius in units of ISCO ($R_{\rm in}$), and outer disk radius in units of gravitational radii ($R_{\rm out}$).

Additionally, we use REFLIONX (Ross & Fabian 2005) to test the robustness of our results obtained with RELXILL and the nature of the Fe K_α line in our BBREFL. In the case of 4U 1636-53, we use a version of REFLIONX[12] that has a variable high energy cut-off. We convolve this model with the relativistic blurring kernel KERRCONV (Brenneman & Reynolds 2006). This provides a completely model-independent check to the values obtained with RELXILL. In the case of GX 17+2 and 4U 1705-44, we have a version of REFLIONX[13] that has been modified to assume a blackbody is illuminating the disk. This reflection model does not represent an independent check on BBREFL since they are derived from the same parent code (Ross & Fabian 1993). It can, however, be used to verify that the Fe K_α line is dynamically broadened and not a result of gas broadening. This is because the REFLIONX model contains additional physics that account for gas effects. It has a broader range of elements, charge states, and ionization while it accounts for the local radiation field at each point. Hence, if we are able to obtain similar values for various parameters, then the line profile is dynamical in origin.

A few reasonable conditions were enforced when making fits with RELXILL and RELCONV. First, we tie the outer emissivity index, $q_{\rm out}$, to the inner emissivity index, $q_{\rm in}$, to create a constant emissivity index. Next, we fix the spin parameter, a_* (where $a_* = cJ/GM^2$), in the model RELCONV to 0.0 and 0.3 in the subsequent fits since NSs in LMXBs have $a_* \leqslant 0.3$ (Miller et al. 2011; Galloway et al. 2008). This does not hinder our estimate of the inner radius since the position of the ISCO is relatively constant for low spin parameters (corrections for frame-dragging for $a_* < 0.3$ give errors $\ll$10%; Miller et al. 1998). Further, the outer disk radius has been fixed to 990 R_g (where $R_g = GM/c^2$). In the case where we use KERRCONV, we tie the emissivity indices to create one emissivity index and fix the outer disk radius to 400 ISCO.

[12] https://www-xray.ast.cam.ac.uk/~mlparker/reflionx_models/reflionx_hc.mod
[13] http://www-xray.ast.cam.ac.uk/~mlparker/reflionx_models/reflionx_bb.mod

3.1. 4U 1636-53

As noted above, initial fits were performed from 3.0 to 50.0 keV with an absorbed cut-off power law to model the continuum emission. Although the continuum is well-described, this model gives a poor fit (χ^2/dof =2435.47/876) since it does not account for the reflection present within the spectrum. A broad Fe K_α line centered ~7 keV with a red wing extending to lower energies and blue wing extending up to 9 keV, implying a high inclination, can be seen in the top panel of Figure 1. The addition of a thermal component improved the overall fit, but the temperature was unfeasibly low for the sensitivity of *NuSTAR* (0.18 ± 0.02 keV) and the normalization was not physically possible ($3.6^{+23.2}_{-3.4} \times 10^7$), hence we excluded it from subsequent modeling.

We performed two fits with TBABS*RELXILL for the different spin values. Each of these provide a significantly better fit (28σ improvement) over the absorbed cut-off power law and can be seen in Table 2. The ionization parameter is reasonable for accreting sources across all fits. The iron abundance is large, but fixing it to lower values does not change the inner disk radius. Regardless of the iron abundance, each fit consistently gives a small inner disk radius of $R_{\rm in} = 1.03 \pm 0.03$ ISCO for $a_* = 0.0$ and $R_{\rm in} = 1.08 \pm 0.06$ ISCO for $a_* = 0.3$. The fit returns a high inclination of 76°.5–79°.9 for each spin value. The photon index is 1.74 ± 0.01 with a cut-off energy at ~20.5 keV. The best-fit spectrum can be seen in Figure 2. Figure 3 shows the goodness of fit versus the inner disk radius (top panel).

To check that the values obtained with our RELXILL modeling of 4U 1636-53 are not model dependent, we apply the model REFLIONX to characterize the emergent reflection spectrum arising from an incident cut-off power-law continuum. We blur the emergent reflection with the relativistic convolution model KERRCONV. This version of REFLIONX has an adjustable cut-off energy, which we tie with the cut-off power law model used to model the continuum emission. This model, however, is angle averaged, unlike RELXILL, which properly takes into account the inclination of the disk when tracing each photon from the disk.

The resulting fit can be seen in Table 3 for a spin of 0.0 and 0.3. The inner disk radius is consistent with the values found in the RELXILL modeling. Additionally, the photon index, high energy cut off, emissivity index, spin parameter, ionization, and inclination are within error for the values found with RELXILL. This demonstrates that the inner disk radius measurement is robust.

3.2. GX 17+2

Initial fits were performed from 3.0–30.0 keV with an absorbed single-temperature blackbody and a multi-temperature blackbody component. This gives a poor fit (χ^2/dof = 4289.59/670) because the reflection spectrum is not yet modeled. The Fe K_α emission can be seen in the middle panel in Figure 1. The red wing extends down to ~4 keV while the blue wing drops around ~7 keV.

We use BBREFL to model the emergent reflection emission and convolve it with RELCONV. The overall model we used was TBABS*(DISKBB+RELCONV*BBREFL). This model provides a better fit with χ^2/dof = 793.2/665 (33σ improvement for the highest χ^2_ν). Parameters and values can be seen in Table 4.

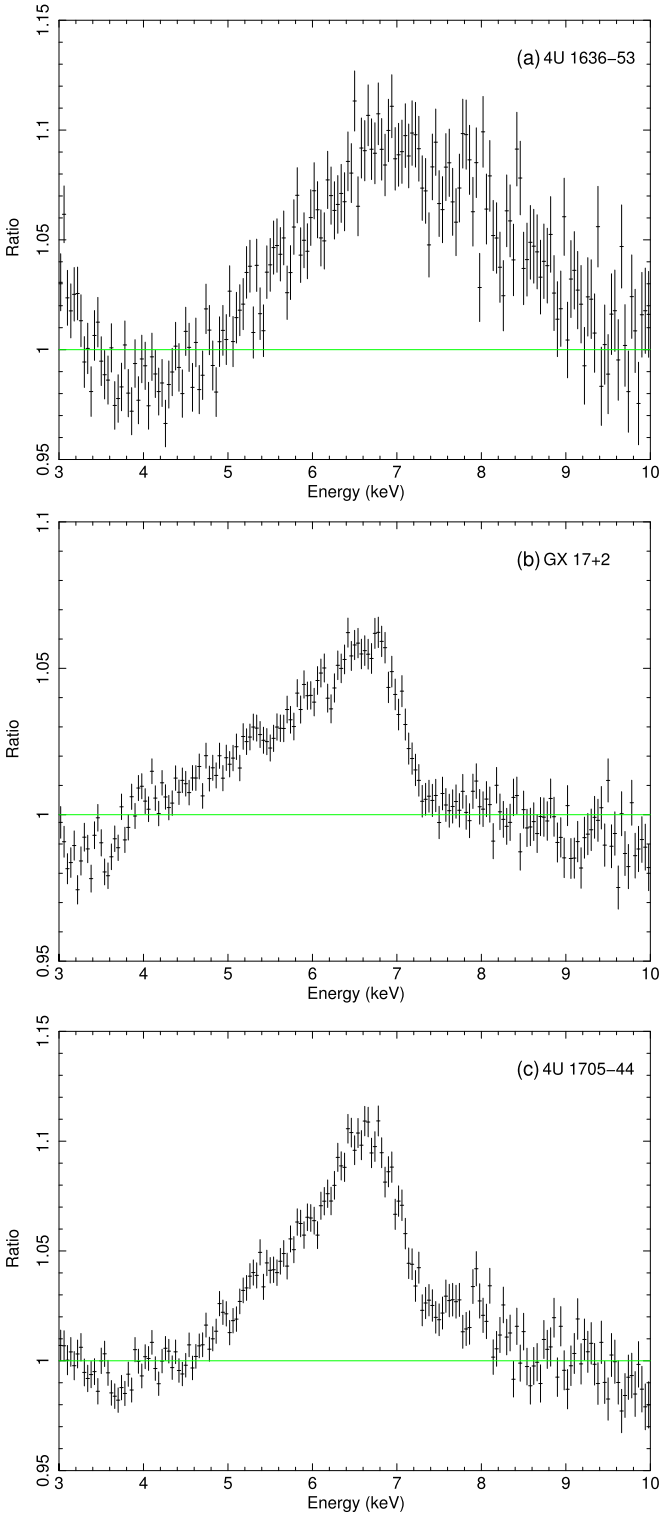

Figure 1. Ratio of the data to the continuum model in the Fe K band for the *NuSTAR* observations of 4U 1636-53, GX 17+2, and 4U 1705-44. The iron line region from 5–8 keV was ignored to prevent the feature from skewing the fit. The data were rebinned for plotting purposes. (a) A simple cut-off power law was fit over the energies of 3.0–5.0 keV and 8.0–50.0 keV. For panels (b) and (c), a simple disk blackbody and single-temperature blackbody was fit over the energies of 3.0–5.0 keV and 8.0–30.0 keV.

Figure 2 shows the best-fit spectrum. For $a_* = 0.0$, the inner disk radius is tightly constrained to $R_{\rm in} = 1.00$–1.02 ISCO for $A_{\rm Fe} = 1.0$ and $R_{\rm in} = 1.00$–1.04 ISCO for $A_{\rm Fe} = 2.0$. For a

Table 2
4U 1636 RELXILL Modeling for Different Spin Parameters

Component	Parameter	RELXILL	
TBABS	$N_{\rm H}$ (10^{22})[a]	0.3	0.3
RELXILL	q	2.25 ± 0.05	2.19 ± 0.04
	a_*[a]	0.0	0.3
	i(°)	78.2 ± 1.67	78.5 ± 1.22
	$R_{\rm in}$ (ISCO)	1.03 ± 0.03	1.08 ± 0.06
	$R_{\rm out}$ (R_g)[a]	990	990
	$R_{\rm in}$ (km)	12.4 ± 0.4	10.8 ± 0.6
	z[a]	0.0	0.0
	Γ	1.74 ± 0.01	1.74 ± 0.01
	log(ξ)	3.3 ± 0.1	3.26 ± 0.06
	$A_{\rm Fe}$	4.9 ± 0.1	4.8 ± 0.1
	$E_{\rm cut}$ (keV)	20.5 ± 0.3	20.5 ± 0.3
	$f_{\rm refl}$	0.42 ± 0.05	0.40 ± 0.04
	norm (10^{-3})	2.21 ± 0.06	2.22 ± 0.03
	$F_{\rm unabs,3.0-50.0\ keV}$	8.9 ± 0.2	8.9 ± 0.1
	$L_{\rm unabs,3.0-50.0\ keV}$	4.6 ± 0.1	4.63 ± 0.06
	$F_{\rm unabs,0.5-50.0\ keV}$	12.8 ± 0.3	12.8 ± 0.2
	$L_{\rm unabs,0.5-50.0\ keV}$	6.7 ± 0.2	6.67 ± 0.09
	χ^2_ν(dof)	1.06 (862)	1.06 (862)

Notes. Errors are quoted at the 1σ confidence level. The absorption column density was fixed to the Dickey & Lockman (1990) value and given in units of cm^{-2}. The spin parameter is pegged at an upper limit of 0.3. The inner disk radius in units of kilometers assumes an NS mass of 1.4 $M_\odot$. Flux is given in units of 10^{-10} erg cm^{-2} s^{-1}. Luminosity is calculated at a maximum of 6.6 kpc and given in units of 10^{36} erg s^{-1}.
[a] Fixed.

higher value of the spin, $a_* = 0.3$, $R_{\rm in} = 1.15^{+0.15}_{-0.08}$ ISCO for $A_{\rm Fe} = 1.0$ and $R_{\rm in} = 1.10 \pm 0.07$ ISCO for $A_{\rm Fe} = 2.0$. The emissivity index is high in each case (ray tracing assuming either a hot spot at a modest latitude or a heated equatorial region, both predict $q = 3.0$; D. Wilkins 2017, private communication). The inclination lies between 25°–38° for all fits. Figure 3 shows the change in goodness of fit versus the inner disk radius (middle panel).

To test the origin of the Fe K$_\alpha$ line, we use a version of REFLIONX that assumes a blackbody is illuminating the accretion disk. Table 4 shows the parameters and values using this model. The overall fit is worse, but still requires a small inner disk radius of $R_{\rm in} = 1.00$–1.02 ISCO for both values of spin. The inclination and ionization is consistent with the values found in previous fits with BBREFL. The emissivity index is close to simple expectations. Regardless, the small inner radii measured with REFLIONX imply that dynamical broadening is dominant in shaping the iron line, and any atmospheric effects are secondary.

3.3. 4U 1705-44

Initial fits were performed from 3.0 to 30.0 keV with an absorbed single-temperature blackbody and a multi-temperature blackbody component. This gives a poor fit (χ^2/dof = 4504.9/670) since the strong disk reflection spectrum has not been modeled. See the bottom panel of Figure 1 for the Fe K$_\alpha$ line.

We use BBREFL to model the emergent reflection emission and convolve it with RELCONV (Dauser et al. 2010). The overall model we used was TBABS*(DISKBB+RELCONV*BBREFL). This

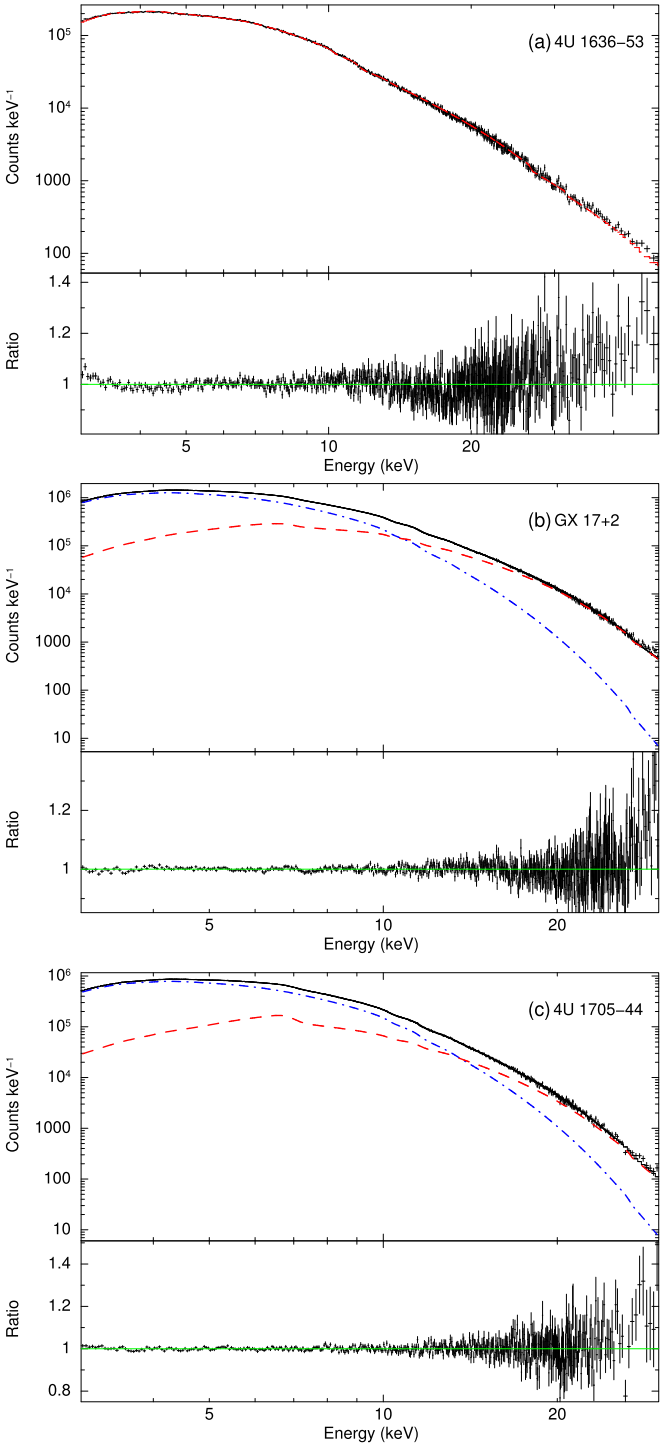

Figure 2. (a) 4U 1636-53 spectrum fit from 3.0–50.0 keV with RELXILL (red dash line) for the fit in Table 2. The panel below shows the ratio of the data to the model. (b) GX 17+2 spectrum fit from 3.0–30.0 keV with DISKBB (blue dot–dash line) and BBREFL (red dash line) for the fit in Table 4. The panel below shows the ratio of the data to the model. (c) 4U 1705-44 spectrum fit from 3.0 to 30.0 keV with DISKBB (blue dot–dash line) and BBREFL (red dash line) for the fit in Table 5. The panel below shows the ratio of the data to the model. The data were rebinned for plotting purposes.

provides a better overall fit (34σ improvement for the highest χ^2_ν). Parameters and values can be seen in Table 5. The inner disk radius is slightly truncated prior to the NS surface between 1.46 and 1.64 ISCO for $a_* = 0.0$ for both values of iron abundance. For $a_* = 0.3$, the inner disk radius is truncated at

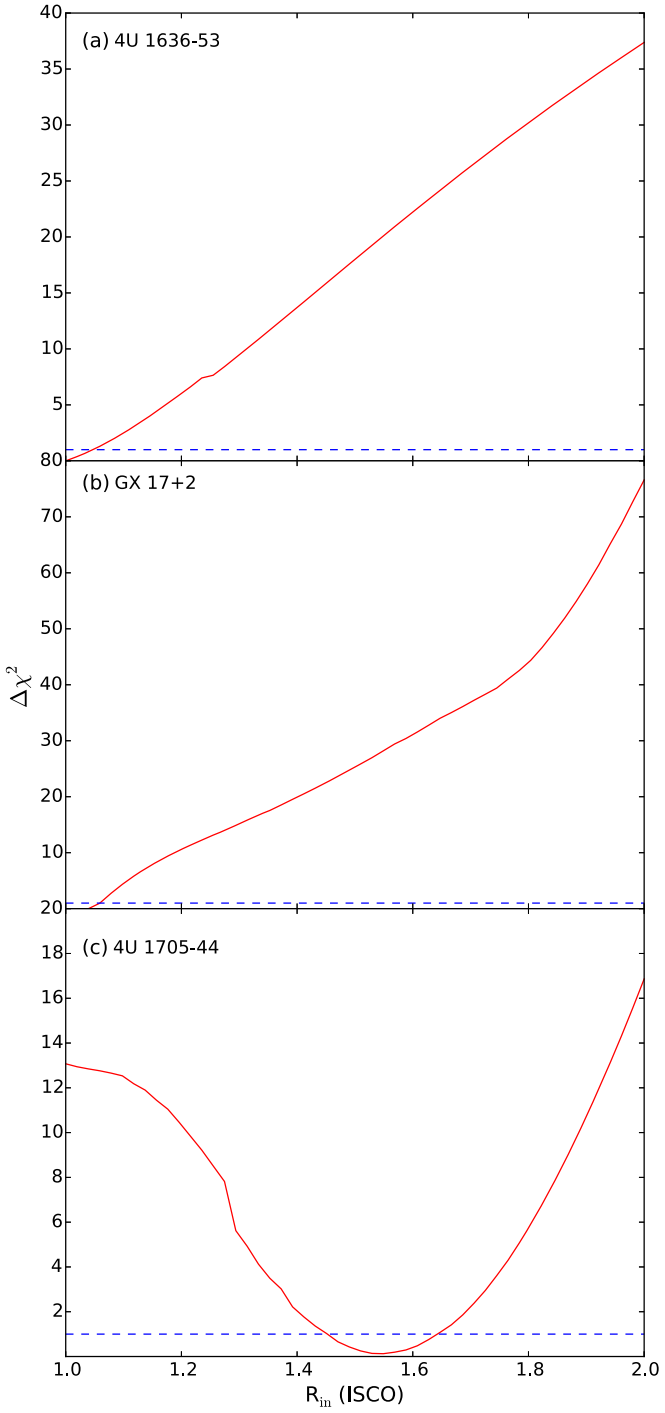

Figure 3. Change in goodness of fit vs. inner disk radius for the *NuSTAR* observations of 4U 1636-53, GX 17+2, and 4U 1705-44 taken over 50 evenly spaced steps generated with XSPEC "steppar." The inner disk radius was held constant at each step while the other parameters were free to adjust. The blue dashed line shows the 68% confidence level. (a) 4U 1636-53 fit corresponding to the first column in Table 2. (b) GX 17+2 fit corresponding to the fifth column in Table 4. (c) 4U 1705-44 fit corresponding to the first column in Table 5.

1.69–1.93 ISCO. The inclination is between 24°.0 and 26°.1 for all fits. The change in goodness of fit versus the inner disk radius can be seen in the bottom panel of Figure 3.

Again, we test the origin of our Fe K_α line in this truncated disk with the version REFLIONX that has been modified for a blackbody illuminating the disk. The resulting fits can be seen

Table 3
4U 1636 REFLIONX Modeling for Different Spin Parameters

Component	Parameter	REFLIONX	
TBABS	N_H (10^{22})[a]	0.3	0.3
CUTOFFPL	Γ	1.74 ± 0.01	1.75 ± 0.01
	E_{cut} (keV)	20.7 ± 0.3	20.6 ± 0.3
	norm	0.20 ± 0.01	0.20 ± 0.01
KERRCONV	q	2.33 ± 0.04	2.28 ± 0.05
	a_*[a]	0.0	0.3
	i(°)	78.6 ± 1.2	78.3 ± 1.2
	R_{in} (ISCO)	1.02 ± 0.02	1.08 ± 0.06
	R_{out} (ISCO)[a]	400	400
	R_{in} (km)	12.2 ± 0.2	10.8 ± 0.6
REFLIONX	ξ	1800 ± 600	1100 ± 500
	A_{Fe}	4.4 ± 0.5	4.6 ± 0.3
	f_{refl}	0.6 ± 0.2	0.6 ± 0.3
	z[a]	0	0
	norm (10^{-7})	2.7 ± 0.9	6.8 ± 4.0
	$F_{unabs,3.0-50.0\ keV}$	9 ± 3	9 ± 5
	$L_{unabs,3.0-50.0\ keV}$	5 ± 2	5 ± 3
	$F_{unabs,0.5-50.0\ keV}$	14 ± 5	14 ± 8
	$L_{unabs,0.5-50.0\ keV}$	7 ± 2	7 ± 4
	χ^2_ν(dof)	1.25 (862)	1.23 (862)

Notes. Errors are quoted at the 1σ confidence level. The absorption column density was fixed to the Dickey & Lockman (1990) value and given in units of cm^{-2}. The spin parameter is pegged at an upper limit of 0.3. The REFLIONX model used has a variable high energy cut off, which we tied to the cut-off energy of the cut-off power law used to model the continuum emission. Additionally, we tied the photon index between REFLIONX and CUTOFFPL. The inner disk radius in units of kilometers assumes an NS mass of 1.4 $M_\odot$. Flux is given in units of 10^{-10} erg cm^{-2} s^{-1}. Luminosity is calculated at a maximum of 6.6 kpc and given in units of 10^{36} erg s^{-1}.
[a] Fixed.

in Table 5. Even though the overall fit is slightly worse, the disk still requires a truncation of $R_{in} = 1.21 \pm 0.18$ ISCO for $a_* = 0.0$ and $R_{in} = 1.37 \pm 0.27$ ISCO for $a_* = 0.3$. Neither model strongly requires that the disk extend to the ISCO, though the ISCO is within 2σ of the nominal best-fit values found with REFLIONX. This confirms that dynamical broadening is the dominant mechanism for the iron line shape.

Since the disk does not extend down to the ISCO, we calculate the extent of a possible boundary layer and place an upper limit on the magnetic field strength since these are plausible scenarios for disk truncation. Popham & Sunyaev (2001) lay out the Newtonian framework for the boundary layer behavior for different mass accretion rates. We estimate the mass accretion for 4U 1705-44 to be $(3.4 \pm 0.4) \times 10^{-9}$ $M_\odot$ yr^{-1} from the 0.5 to 30.0 keV unabsorbed luminosity and using an efficiency of $\eta = 0.2$ (Sibgatullin & Sunyaev 2000). Using Equation (25) in Popham & Sunyaev (2001), we estimate that the boundary layer extends out to ~1.2 ISCO (assuming 1.4 $M_\odot$ and $a_* = 0.0$). Additional factors, such as spin and viscosity in the layer, can extend this region to be consistent with the truncation of the inner disk.

If the disk is impeded by the magnetosphere, we can place an upper limit on the strength of the field using the upper limit of $R_{in} = 9.8\ R_g$. Assuming a mass of 1.4 $M_\odot$, taking the distance to be 7.8 kpc, and using the unabsorbed flux from 0.5 to 30.0 keV of 5.2×10^{-9} erg cm^{-2} s^{-1} as the bolometric flux, we can determine the magnetic dipole moment, μ, from

Table 4
GX 17+2 Reflection Modeling

Component	Parameter	BBREFL				REFLIONX	
TBABS	$N_{\rm H}$ (10^{22})[a]	0.9	0.9	0.9	0.9	0.9	0.9
DISKBB	$T_{\rm in}$	1.93 ± 0.04	1.992 ± 0.001	1.93 ± 0.05	1.92 ± 0.06	1.92 ± 0.01	1.92 ± 0.01
	norm	26 ± 1	23.8 ± 0.1	26 ± 2	26 ± 2	26.8 ± 0.4	26.7 ± 0.4
BLACKBODY	*kT*	…	…	…	…	2.86 ± 0.01	2.86 ± 0.01
	norm (10^{-2})	…	…	…	…	2.9 ± 0.1	2.9 ± 0.1
RELCONV	q	$8.1^{+0.8}_{-1.0}$	$3.7^{+4.7}_{-0.3}$	6.0 ± 3.0	4.5 ± 1.5	3.5 ± 0.1	3.2 ± 0.1
	a_*[a]	0.0	0.3	0.0	0.3	0.0	0.3
	i(°)	$35.1^{+0.2}_{-0.6}$	30^{+8}_{-2}	30 ± 5	30 ± 4	25.9 ± 0.2	25.8 ± 0.2
	$R_{\rm in}$ (ISCO)	$1.00^{+0.02}$	$1.15^{+0.15}_{-0.08}$	1.02 ± 0.02	1.10 ± 0.07	1.01 ± 0.01	1.01 ± 0.01
	$R_{\rm out}$ (R_g)[a]	990	990	990	990	990	990
	$R_{\rm in}$ (km)	$12.0^{+0.2}$	$11.5^{+1.5}_{-0.8}$	12.2 ± 0.2	11.0 ± 0.7	12.1 ± 0.1	10.1 ± 0.1
BBREFL	$\log(\xi)$	$2.47^{+0.07}_{-0.01}$	2.45 ± 0.01	$2.33^{+0.09}_{-0.01}$	2.40 ± 0.06	…	…
	kT (keV)	$3.15^{+0.01}_{-0.07}$	$3.12^{+0.04}_{-0.01}$	$3.03^{+0.05}_{-0.01}$	3.03 ± 0.02	…	…
	$A_{\rm Fe}$[a]	1.0	1.0	2.0	2.0	…	…
	$f_{\rm refl}$	$1.69^{+0.04}_{-0.67}$	$1.52^{+0.67}_{-0.01}$	$1.2^{+0.2}_{-0.4}$	$1.27^{+0.04}_{-0.50}$	…	…
	z[a]	0	0	0	0	…	…
	norm (10^{-26})	$8.83^{+0.60}_{-0.01}$	$8.61^{+0.02}_{-0.36}$	$13.0^{+1.0}_{-0.03}$	$13.1^{+0.08}_{-0.01}$	…	…
REFLIONX	ξ	…	…	…	…	240 ± 20	230 ± 7
	$A_{\rm Fe}$	…	…	…	…	2.1 ± 0.4	2.1 ± 0.4
	$f_{\rm refl}$	…	…	…	…	0.9 ± 0.1	0.9 ± 0.1
	z[a]	…	…	…	…	0	0
	norm	…	…	…	…	1.7 ± 0.2	1.8 ± 0.1
	$F_{\rm unabs,3.0-30.0\ keV}$	$7.3^{+0.6}_{-0.3}$	$7.30^{+0.04}_{-0.31}$	$7.3^{+0.8}_{-0.6}$	7.3 ± 0.1	7.3 ± 0.9	7.3 ± 0.5
	$L_{\rm unabs,3.0-30.0\ keV}$	1.5 ± 0.1	$1.48^{+0.01}_{-0.06}$	$1.5^{+0.2}_{-0.1}$	1.48 ± 0.02	1.5 ± 0.2	1.5 ± 0.1
	$F_{\rm unabs,0.5-30.0\ keV}$	$10.7^{+0.8}_{-0.4}$	$10.7^{+0.1}_{-0.4}$	$10.7^{+1.2}_{-0.8}$	10.7 ± 0.8	11.0 ± 1.3	11.0 ± 0.7
	$L_{\rm unabs,0.5-30.0\ keV}$	$2.2^{+0.2}_{-0.1}$	$2.16^{+0.01}_{-0.08}$	2.2 ± 0.2	2.2 ± 0.2	2.2 ± 0.3	2.2 ± 0.1
	χ^2_ν(dof)	1.06 (665)	1.13 (665)	1.19 (665)	1.18 (665)	1.28 (664)	1.26 (664)

Notes. Errors are quoted at the 1σ confidence level. The absorption column density was fixed to the Dickey & Lockman (1990) value and given in units of $\rm cm^{-2}$. Limb brightening was assumed. The emissivity index was pegged at the hard limit of 3.0. The REFLIONX model used has been modified for a blackbody illuminating the accretion disk. The inclination for REFLIONX was pegged within the limits found with BBREFL, due to the model being angle averaged and not able to constrain the inclination. The ionization parameter was also pegged within the BBREFL values since it was unconstrained on its own. The blackbody temperature in REFLIONX was tied to the temperature of the blackbody used to model the continuum emission. The emissivity index was pegged at the hard limit of 3.0. The inner disk radius in units of kilometers assumes an NS mass of 1.4 $M_\odot$. Flux is given in units of 10^{-9} erg $\rm cm^{-2}$ $\rm s^{-1}$. Luminosity is calculated at a maximum of 13.0 kpc and given in units of 10^{38} erg $\rm s^{-1}$.
[a] Fixed.

Equation (1) taken from Cackett et al. (2009). If we make the same assumptions about geometry (i.e., $k_A = 1$, $f_{\rm ang} = 1$) and use an accretion efficiency of $\eta = 0.2$, then $\mu \simeq 2.2 \times 10^{26}$ G $\rm cm^3$. This corresponds to a magnetic field strength of $B \simeq 4.3 \times 10^8$ G at the magnetic poles for an NS of 10 km. Moreover, if we assume a different conversion factor $k_A = 0.5$ (Long et al. 2005) then the magnetic field strength at the poles would be $B \simeq 1.5 \times 10^9$ G. Note that the magnetic field strength at the pole is twice as strong as at the equator. However, the type 1 X-ray burst that occurred during the observation means material is still reaching the surface of the NS and no pulsations have been seen.

4. Discussion

Using *NuSTAR*, we have taken a hard look at three well-known NS X-ray binaries. Our observations captured 4U 1636−53 in the hard state, while GX 17+2 and 4U 1705−44 were caught in soft states. Owing to *NuSTAR*'s broad bandpass and its ability to measure robust spectra at high flux levels, we are able to constrain different properties of these sources through modeling of reflection from their disks. Different disk reflection spectra are considered for each source in order to examine how inferred radii depend on modeling assumptions. For plausible combinations of NS masses and dimensionless angular momenta, our results imply that disks extend to an ISCO, that NSs are smaller than their ISCO, and the results begin to place meaningful constraints on NS radii. In this section, we consider the results within the context of the NS EOS, implications for the inner accretion flow onto NSs, and evaluate possible systematic errors and avenues for improvement in future studies.

4.1. NS Radius Constraints

4U 1636-53 is found to have an inner disk radius of 1.00–1.03 ISCO for $a_* = 0.0$ and 1.02–1.14 ISCO for $a_* = 0.3$ as constrained from RELXILL modeling of the reflection spectrum. We applied another reflection model, REFLIONX, to test the robustness of our measurement. The resulting fit gave a nearly identical inner disk measurement. For $a_* = 0.3$ and 1.4 $M_\odot$, 1.08 ± 0.06 ISCO translates to 10.8 ± 0.6 km. For the lower value of $a_* = 0.0$ and 1.4 $M_\odot$, 1.03 ± 0.03 ISCO translates to 12.4 ± 0.4 km. This small

Table 5
4U 1705-44 Reflection Modeling

Component	Parameter	BBREFL				REFLIONX	
TBABS	$N_{\rm H}$ (10^{22})[a]	0.7	0.7	0.7	0.7	0.7	0.7
DISKBB	$T_{\rm in}$	2.13 ± 0.01	2.13 ± 0.01	2.00 ± 0.01	2.00 ± 0.01	1.95 ± 0.02	1.95 ± 0.03
	norm	9.65 ± 0.02	9.6 ± 0.1	11.48 ± 0.02	11.60 ± 0.01	12.3 ± 0.5	12.4 ± 0.6
BLACKBODY	*kT*	...	...	...	...	2.54 ± 0.02	2.54 ± 0.03
	norm (10^{-2})	...	...	...	...	1.15 ± 0.05	1.15 ± 0.08
RELCONV	*q*	3.1 ± 0.1	3.1 ± 0.1	3.2 ± 0.1	3.2 ± 0.1	2.8 ± 0.3	2.7 ± 0.3
	a_*[a]	0.0	0.3	0.0	0.3	0.0	0.3
	i(°)	24.4 ± 0.4	24.4 ± 0.4	24.6 ± 0.5	25.6 ± 0.5	13 ± 11	16 ± 6
	$R_{\rm in}$ (*ISCO*)	1.54 ± 0.08	1.82 ± 0.09	1.50 ± 0.07	1.78 ± 0.09	1.21 ± 0.18	1.37 ± 0.27
	$R_{\rm out}$ (R_g)[a]	990	990	990	990	990	990
	$R_{\rm in}$ (*km*)	18.4 ± 1.0	18.2 ± 0.9	18.0 ± 0.8	17.8 ± 0.9	14.5 ± 2.2	13.7 ± 2.7
BBREFL	log(ξ)	2.67 ± 0.02	2.66 ± 0.02	2.74 ± 0.04	2.74 ± 0.04	...	...
	kT (keV)	2.83 ± 0.01	2.84 ± 0.02	2.67 ± 0.01	2.67 ± 0.01	...	...
	$A_{\rm Fe}$[a]	1.0	1.0	2.0	2.0	...	...
	$f_{\rm refl}$	2.0 ± 0.1	2.1 ± 0.2	0.74 ± 0.02	0.74 ± 0.02	...	...
	z[a]	0	0	0	0	...	...
	norm (10^{-26})	1.24 ± 0.06	1.24 ± 0.08	2.1 ± 0.2	2.1 ± 0.2	...	...
REFLIONX	ξ	...	...	...	...	430 ± 20	430 ± 20
	$A_{\rm Fe}$	...	...	...	...	2.0 ± 0.4	2.0 ± 0.6
	$f_{\rm refl}$	...	...	...	...	0.72 ± 0.06	0.72 ± 0.08
	z[a]	...	...	...	...	0	0
	norm	...	...	...	...	0.57 ± 0.04	0.60 ± 0.05
	$F_{\rm unabs,3.0-30.0\ keV}$	3.4 ± 0.2	3.4 ± 0.2	3.4 ± 0.3	3.4 ± 0.3	3.4 ± 0.3	3.4 ± 0.4
	$L_{\rm unabs,3.0-30.0\ keV}$	2.5 ± 0.1	2.5 ± 0.2	2.5 ± 0.2	2.5 ± 0.2	2.5 ± 0.2	2.5 ± 0.3
	$F_{\rm unabs,0.5-30.0\ keV}$	5.0 ± 0.2	5.0 ± 0.3	5.0 ± 0.5	5.0 ± 0.5	5.2 ± 0.5	5.2 ± 0.6
	$L_{\rm unabs,0.5-30.0\ keV}$	3.7 ± 0.2	3.7 ± 0.2	3.7 ± 0.3	3.7 ± 0.3	3.8 ± 0.3	3.8 ± 0.5
	χ^2_ν(dof)	1.16 (665)	1.16 (665)	1.19 (665)	1.19 (665)	1.21 (664)	1.21 (664)

Notes. Errors are quoted at the 1σ confidence level. The absorption column density was fixed to the Dickey & Lockman (1990) value and given in units of cm^{-2}. Limb brightening was assumed. The REFLIONX model used has been modified for a blackbody illuminating the accretion disk. The inclination for REFLIONX was pegged within the limits found with the BBREFL, due to the model being angle averaged and not able to constrain the inclination. The ionization parameter was also pegged within the BBREFL values since it was unconstrained on its own. The blackbody temperature in REFLIONX was tied to the temperature of the blackbody used to model the continuum emission. The inner disk radius in units of kilometers assumes an NS mass of 1.4 $M_\odot$. Flux is given in units of 10^{-9} erg cm^{-2} s^{-1}. Luminosity is calculated at a maximum of 7.8 kpc and given in units of 10^{37} erg s^{-1}.
[a] Fixed.

Table 6
NS Inner Disk Radii and Eddington Fraction Observed with *NuSTAR*

Source	$R_{\rm in}$ (ISCO)	$F_{\rm Edd}$	References
Ser X-1	1.03–1.20	0.34	1
4U 1705-44	1.46–1.93	0.10	...
4U 1636-53	1.00–1.14	0.01	...
GX 17+2	1.00–1.30	0.57	...
RXS J1804	1.00–1.85	0.02	2
	1.0–1.5	0.10	3
Aql X-1	2.31–3.46	0.13	4
4U 1608-52	1.3–2.0	0.03	5
4U 1728-34	1.0–2.0	0.04	6

References. (1) Miller et al. (2013), (2) Ludlam et al. (2016), (3) Degenaar et al. (2016), (4) King et al. (2016), (5) Degenaar et al. (2015), (6) Sleator et al. (2016).

inner disk radius is in agreement with previous measurements for this source that were consistent with the ISCO (Pandel et al. 2008; Cackett et al. 2010; Sanna et al. 2013). The high inclination of 4U 1636-53 is consistent with previous reflection studies (Frank et al. 1987; Casares et al. 2006; Cackett et al. 2010; Sanna et al. 2013).

Similarly, the inner disk radius in GX 17+2 is tightly constrained to 1.00–1.02 ISCO for $a_* = 0.0$ and 1.03–1.30 ISCO for $a_* = 0.3$ by using the blackbody reflection model BBREFL. We found a tighter constraint on the inner disk radius of 1.00–1.01 ISCO when we applied a REFLIONX model that was modified for a blackbody illuminating the disk. For $a_* = 0.0$ and 1.4 $M_\odot$, 1.00–1.02 ISCO translates to 12.0–12.2 km. For the higher value of $a_* = 0.3$ and 1.4 $M_\odot$, 1.03–1.30 ISCO translates to 10.3–13 km. The inclination was found to be 25°–38°. Cackett et al. (2010) found similarly small inner disk radii and low inclination for this system.

Thus, in the most sensitive and robust spectra of 4U 1636 −53 and GX 17+2 yet obtained, the innermost extent of the accretion disk is found to be close to the ISCO, with consequences for the NS radii. There may still be a boundary layer present on the surface of the NS, but in this case it would have to be quite small. Given that 1 ISCO corresponds to 12 km, for $a_* = 0$ and 1.4 $M_\odot$, and using the fiducial NS radius of 10 km, the boundary layer would be about ∼2 km. The inner disk radii are not strongly dependent upon the reflection models that are utilized. We therefore proceed to examine the implications of the results for the EOS of ultradense matter in a more generalized way. Rather than assuming specific

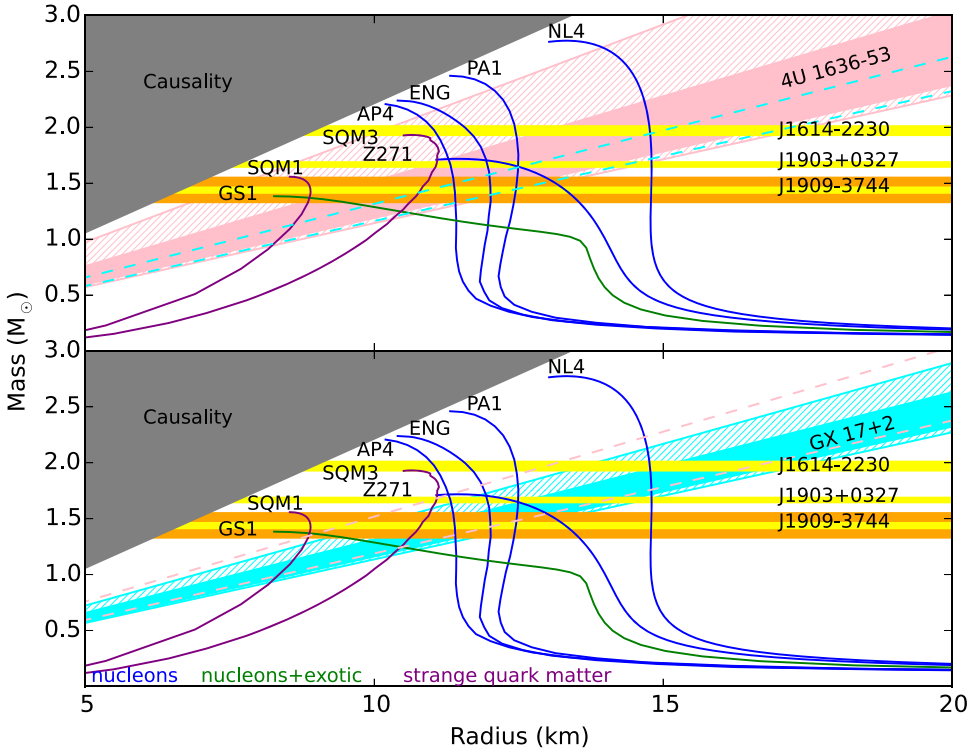

Figure 4. Constraints on the cold, ultradense matter equation of state from Fe K_α reflection modeling to determine the inner disk radius, assuming that the stellar surface is truncating the disk. The gray region is excluded by causality (the speed of sound must be less than the speed of light). The curve labeled NL4 is from Akmal et al. (1998) and Z271 is from Horowitz & Piekarewicz (2001). All other mass–radius curves are labeled as in Lattimer & Prakash (2001). The shaded regions for 4U 1636-53 and GX 17+2 correspond to the allowed values for mass and radius given a spin frequency of 518.0 Hz (Galloway et al. 2008) and 293.2 Hz (Wijnands et al. 1997), respectively. For reasonable values of mass and radius, a spin frequency of 518.0 Hz relates to a spin parameter of $0.09 \pm 0.05 < a_* < 0.44 \pm 0.23$ and 293.2 Hz gives $0.05 \pm 0.04 < a_* < 0.25 \pm 0.13$. The hatched area represents the errors on the spin parameter. The dashed lines in each panel represent the solid area constraints from the NS in the other panel. The yellow horizontal lines are the measured masses for the NSs PSR J1614-2230 ($M = 1.97 \pm 0.04\ M_\odot$; Demorest et al. 2010), PSR 1903+0327 ($M = 1.667 \pm 0.021\ M_\odot$; Freire et al. 2011), and PSR J1909-3744 ($M = 1.438 \pm 0.024\ M_\odot$; Jacoby et al. 2005). The orange region represents the mass range found for an NS in a double NS system ($M = 1.33$–$1.55\ M_\odot$; see Kiziltan et al. 2013 for a review).

values $a = cJ/GM^2$, we need to determine the likely range of a given the measured spin frequencies for these sources.

4U 1636-53 and GX 17+2 have known rotation frequencies $\nu_{1636-53} = 518.0$ Hz (Galloway et al. 2008) and $\nu_{17+2} = 293.2$ Hz (Wijnands et al. 1997), respectively. The total angular momentum, J, can be obtained from the spin frequency assuming a reasonable range of mass and radius for an NS and a solid sphere ($J = \frac{2}{5} MR^2\omega$ where $\omega = 2\pi\nu_{\rm spin}$). For 4U 1636−53, $\nu = 518$ Hz then implies $0.09 \pm 0.05 < a_{1636-53} < 0.44 \pm 0.23$, and $\nu = 293.2$ Hz implies $0.05 \pm 0.04 < a_{17+2} < 0.25 \pm 0.13$. These values assume a mass range of $1.3 \leqslant M_{\rm NS}/M_\odot \leqslant 2.1$, consistent with the range of masses that have been measured directly (Jacoby et al. 2005; Demorest et al. 2010; Freire et al. 2011; Kiziltan et al. 2013). The lower limit of the radius range was determined by where causality approximately intersects the largest measured NS. The upper limit of the radius range was limited by break up ($a_* = 0.7$).

The radius of the ISCO around a compact object in units of gravitational radii is depends on its spin (Bardeen et al. 1972); the ranges above therefore enable a translation to gravitational radii and then into kilometers. Figure 4 plots these ranges in the mass versus radius plane used to characterize the EOS. Several equations of states from Akmal et al. (1998), Lattimer & Prakash (2001), and Horowitz & Piekarewicz (2001) are also plotted, as well as known NS masses from pulsar timing methods and binaries. The regions allowed by our models must be considered upper limits on the radius of NSs, since the NS can be smaller than its ISCO. Disk reflection is not yet able to rule out plausible EOSs; however, deeper X-ray spectra and/or mass measurements in these systems can greatly reduce the allowed regions in this mass–radius plane.

4.2. Implications of Disk Truncation in 4U 1705−44

In 4U 1636−53 and GX 17+2, the inner disk appears to extend to the ISCO, and we cannot place any constraints on the magnetic field in these sources. In contrast, 4U 1705-44 has an inner disk radius of 1.46–1.64 ISCO for $a_* = 0.0$ and 1.69–1.93 ISCO for $a_* = 0.3$. For a spin of 0.0 and stellar mass of 1.4 $M_\odot$, 1.46–1.64 ISCO translates to 17.5–19.7 km. For a spin of 0.3 and stellar mass of 1.4 $M_\odot$, 1.69–1.93 ISCO translates into 16.9–19.3 km.

The similarity between the results of our fits and prior work suggests that such modeling is converging on a relatively consistent set of physical constraints. A truncated disk has been indicated in 4U 1705−44 in several prior investigations (di Salvo et al. 2009; Reis et al. 2009b; Cackett et al. 2010, 2012; Egron et al. 2013; Di Salvo et al. 2015). Our results closely match those of Reis et al. (2009b); that work reported the disk of 4U 1705−44 was truncated above the stellar surface with a gap of ∼3.5 km. Our models find that the inclination of the inner disk is between 24°.0 and 26°.1; this is again largely consistent with previous reflection studies (20°–50°, Piraino et al. 2007; ⩽35°, Reis et al. 2009b; D'Aì et al. 2010;

Cackett et al. 2010, 2012; Egron et al. 2013). Di Salvo et al. (2015) find a slightly larger inclination than we do of $43^\circ \pm 5^\circ$.

Disks around NSs can be truncated by a boundary layer or by magnetic pressure. It is also possible that the inner disk may evaporate at low accretion rates, qualitatively similar to the expected truncation of disks around BHs at low mass-accretion rates. Evidence of this may be seen in *HETE* J1900.1-2455 (Papitto et al. 2013).

In Section 3.3, we estimated that the boundary layer could push out to 1.2 ISCO based on the arguments in Popham & Sunyaev (2001). This is smaller than the radius implied by most of our disk reflection models, but the predicted extent of the boundary layer can be increased for specific combinations of radiative efficiency and stellar spin. D'Aì et al. (2010) estimated that the boundary layer in 4U 1705−44 extended out to $\sim 2\ R_{\rm NS}$ in the soft state. Our estimate is consistent with this picture assuming an NS radius of 10 km.

If the NS magnetosphere is truncating the disk, we place an upper limit on the magnetic field strength at the poles to be $B \leqslant (0.4\text{–}1.5) \times 10^9$ (see Section 3.3). A recent study by King et al. (2016) also found a truncated disk surrounding the well-known NS X-ray binary and pulsar Aql X-1. An inner disk radius of $R_{\rm in} = 15 \pm 3\ R_g = 2.88 \pm 0.58$ ISCO was measured via disk reflection. If the disk was not truncated by a boundary layer and instead by the NS magnetic field, an upper limit of $B < 5 \pm 2 \times 10^8$ G results (King et al. 2016). Aql X-1 had a type 1 X-ray burst during the observation, suggesting that some material was still reaching the surface, like 4U 1705−44.

4.3. Inner Accretion Flows and $\dot{M}$

It is expected that the inner radius of an accretion disk is partly set by the mass accretion rate through the disk (see, e.g., González Martínez-País et al. 2014). Indeed, as noted above, several mechanisms might truncate the inner accretion disk around an NS, but each truncation mechanism becomes more effective at lower mass-accretion rates. Indeed, the radial extent of the inner disk may be an important factor in determining the phenomena manifested in different parts of the "Z" and "atoll" tracks followed by many persistent NS X-ray binaries and even the position of the source along such tracks.

The sensitive spectra that we have obtained with *NuSTAR* have permitted particularly strong radius constraints. Prior *NuSTAR* observations of NSs have also measured inner disk radii. It is now pragmatic to consider what a modest collection of robust spectral constraints implies about the evolution of the inner accretion disk around NSs as a function of the mass accretion rate. For consistency, we carefully replicated the models considered in prior work within XSPEC and extrapolated the models to a common energy range (0.5–50 keV). We then use the maximum distance to each source to convert unabsorbed fluxes to luminosities, and divided by an Eddington limit of 3.8×10^{38} erg s^{-1} as per Kuulkers et al. (2003) to obtain the Eddington fraction.

Table 6 lists the key data that result from this exercise. Figure 5 plots the inner disk radius versus Eddington fraction for a set of eight NSs observed with *NuSTAR*. Across almost two orders of magnitude in Eddington fraction—implying an equivalent range in mass accretion rate if the efficiency is independent—the inner disk appears to remain very close to the ISCO. The most obvious exception to the overall trend is Aql X-1; however, this source is known to be a pulsar and it may have a slightly higher magnetic field than other sources in the sample.

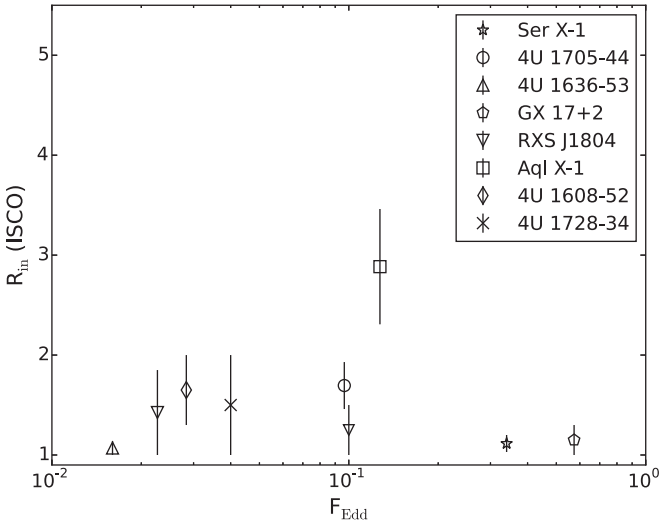

Figure 5. Comparison of Eddington fraction and measured inner disk radii for NSs observed with *NuSTAR*. Inner disk radius and Eddington fractions for 4U 1608-52, Ser X-1, Aql X-1, and 4U 1728-34 are obtained from Degenaar et al. (2015), Miller et al. (2013), King et al. (2016), and Sleator et al. (2016), respectively. Values for RXS J1804 are taken from Ludlam et al. (2016) and Degenaar et al. (2016). See Table 6 for inner disk radii and Eddington fractions.

Cackett et al. (2010) found similar results when looking at the inner disk radius dependence on Eddington fraction for a sample of 10 NSs that were observed with *XMM-Newton* and *Suzaku*. Chiang et al. (2016) recently looked at *Suzaku* observations of Ser X-1 over a range of flux states and found that the inner disk radius changes little between 0.2–0.6 $L_{\rm Edd}$. Disk reflection studies undertaken with *NuSTAR* have the advantages of a broad, continuous bandpass that enables better characterization of the direct continuum and stronger constraints on the total reflection spectrum, and spectroscopy that is not distorted by photon pile-up (which can falsely skew the shape of the line: Miller et al. 2010; Ng et al. 2010).

4.4. Potential Systematic Errors and Modeling Issues

We have obtained spectra with very high statistical quality, and therefore spectral fitting results with small statistical errors. Systematic errors are likely to be comparable or larger, and should be considered. In practice, the most important sources of systematic errors are difficult to quantify, but they are important to mention.

All measures of BH spin that utilize the accretion disk, and all limits on NS radii that utilize the disk (including disk reflection and QPOs), assume that gas in the disk orbits as test particles would orbit. If real fluid disks push slightly inward of the ISCO defined for test particles, it amounts to a systematic error on such measurements. There is no astrophysical test of this assumption, but numerical simulations can potentially provide some insights. Explorations of disks around BHs suggest that accretion disks do generally obey the test particle ISCO (Reynolds & Fabian 2008). Similar simulations have not been performed in the presence of an NS, and the influence of a boundary layer may also induce small changes. New simulations can help to address such systematics.

Apart from the reaction of the accretion disk to the potential, it is possible that our assumption of a Kerr metric is itself a source of systematic error. The NS that we have studied may

have small quadrupole moments, and this could change the effective potential in which the disk orbits. One treatment suggests that systematic errors related to quadrupole-induced deviations from a pure Kerr metric are $\leqslant$10% even for a dimensionless spin parameter of $a = 0.3$ (Sibgatullin & Sunyaev 1998).

The blurred reflection models themselves can potentially be sources of systematic error. Some ancillary parameters of the reflection models require a note of caution. We now turn to these issues.

For 4U 1636−53, both RELXILL and RELCONV×REFLIONX return small and formally consistent inner disk radii. Different runs with RELCONV×BBREFL and RELCONV×REFLIONX all return small radii consistent with $R_{\rm in} \leqslant 1.1$ ISCO in fits to GX 17+2. In some cases, the errors are formally different at the 1σ level of confidence, but the values are consistent over more conservative ranges. In these two cases, the models are in close agreement and suggest that the radius values that emerge can be taken seriously. For 4U 1705−44, a greater range of inner disk radii emerges with different models and parameter selections. The most recent model, REFLIONX, returns radii that are nearly consistent with the ISCO at 1σ; other models return values as large as $R_{\rm in} = 1.8$ ISCO, and the majority of models—and the best overall fits—measure a truncated disk. Deeper observations of 4U 1705−44 may be required to obtain a more definitive picture of that source.

The emissivity profile of the accretion disk encodes the geometry of the emitting source and spacetime of the innermost environment. An emissivity index of $q = 3$ is expected for a point source emitter in a (nearly) Schwarzschild spacetime, and different plausible geometries for NSs (boundary layers, hot spots) appear to produce the same emissivity profile (D. Wilkins 2017, private communication). Both families of reflection models prefer a flatter emissivity in fits to the spectrum of 4U 1636−53. This may be the result of a more extended corona in the hard state. Fits to the spectrum of GX 17+2 with BBREFL generally prefer a much steeper index, but fits with the more recent REFLIONX model are only slightly steeper than $q = 3$. This is broadly consistent with the direct continuum, which suggests that a boundary layer or hot spot is likely irradiating the disk. The models for 4U 1705−44 are all broadly consistent with $q = 3$.

The abundance of iron affects the local *strength* of reflection relative to the direct continuum, not the shape of the line. It is the *shape* of the disk reflection spectrum—and particularly the shape of the Fe K emission line—that is used to infer the inner radius of the accretion disk, and to thereby set an upper limit on the radius of the NS. The abundance of iron does not directly affect our radius measurements. However, it is interesting to consider this parameter and whether or not it is accurately determined. Both families of reflection models prefer an iron overabundance of 4.5–5.0 relative to solar values, in fits to 4U 1636−53. It is unlikely that the abundance of iron is that high in the low mass companion star in 4U 1636−53, but it is possible that this measurement correctly describes the atmosphere of the accretion disk. There, the ionization structure may skew the relative abundances of different elements to values that do not reflect the overall abundances within the accretion flow. Fits to the spectra of GX 17+2 and 4U 1705−44 are consistent with iron abundances of 1.0–2.0 times solar values, but these fits also return lower ionization parameters, potentially consistent with ionization affecting abundance measurements. It is also possible that the enhanced abundances may be the result of effects in especially dense gas. In these cases, the abundance would increase to replicate the continuum for a lower density disk allowed by the atomic data set within the current reflection models (García et al. 2016).

Finally, we simply note that the ionization parameters measured in different fits to each source spectrum are comparable to the values seen for other NS reflection studies, $2.3 < \log(\xi) < 4.0$ (Cackett et al. 2010; Miller et al. 2013; Degenaar et al. 2015).

5. Conclusions

We have measured the inner disk radius for three different NSs that were observed with *NuSTAR*. 4U 1636-53 and GX 17 +2 have a small inner disk radius that is constrained to the ISCO. This value has proven to be model independent for 4U 1636-53 and suggest that the NS is smaller than their ISCO. Converting ISCO to kilometers for a range of spin parameters and NS masses provides a range in which allowed theoretical EOSs must lie. 4U 1705-44 possesses a truncated disk which we used to explore the possibility of a magnetic field or a boundary layer. We estimate the upper limit of the magnetic field surrounding the NS to be $B \leqslant (0.4 - 1.5) \times 10^9$ G at the poles and depends on assumed conversion factor between disk and spherical accretion. We estimate the extent of a possible boundary layer out to ∼1.2 ISCO.

Disk reflection has proven to be a valuable tool in determining properties of NSs, such as limits on the extent of the NS radius, boundary layer, and magnetic field strength. It provides another method to narrow down the elusive EOS of ultradense, cold matter that makes up the NS. The advantage of this method is that the distance to the source is not needed and short observations can provide a clear look at Fe K_α emission. Furthermore, complementary mass estimates can yield further constraints to the EOS.

This research has made use of the *NuSTAR*. Data Analysis Software (NuSTARDAS) jointly developed by the ASI Science Data Center (ASDC, Italy) and the California Institute of Technology (Caltech, USA). J.M.M. gratefully acknowledges support through the *NuSTAR* guest observer program. N.D. is supported via an NWO Vidi grant and an EU Marie Curie Intra-European fellowship under contract no. FP-PEOPLE-2013-IEF-627148. E.M.C. gratefully acknowledges support from the National Science Foundation through CAREER award number AST-1351222.

References

Akmal, A., Pandharipande, V. R., & Ravenhall, D. G. 1998, PhRvC, 58, 1804
Arnaud, K. A. 1996, in ASP Conf. Ser 101. Astronomical Data Analysis Software and Systems V, ed. G. H. Jacoby & J. Barnes (San Francisco, CA: ASP), 17
Ballantyne, D. R. 2004, MNRAS, 351, 57
Bardeen, J. M., Press, W. H., & Teukolsky, S. A. 1972, ApJ, 178, 347
Barret, D., & Olive, J.-F. 2002, ApJ, 576, 391
Barret, D., Olive, J.-F., & Miller, M. C. 2006, MNRAS, 370, 1140
Bhattacharyya, S., & Strohmayer, T. E. 2007, ApJL, 664, L103
Brenneman, L. W., & Reynolds, C. S. 2006, ApJ, 652, 1028
Cackett, E. M., Altamirano, D., Patruno, A., et al. 2009, ApJL, 694, L21
Cackett, E. M., Miller, J. M., Reis, R. C., Fabian, A. C., & Barret, D. 2012, ApJ, 755, 27
Cackett, E. M., Miller, J. M., Bhattacharyya, S., et al. 2008, ApJ, 674, 415
Cackett, E. M., Miller, J. M., Ballantyne, D. R., et al. 2010, ApJ, 720, 205
Callanan, P. J., Curran, P., Filippenko, A. V., et al. 2002, ApJL, 574, L143
Casares, J., Cornelisse, R., Steeghs, D., et al. 2006, MNRAS, 373, 1235

Cash, W. 1979, ApJ, 228, 939
Chiang, C.-Y., Morgan, R. A., Cackett, E. M., et al. 2016, ApJ, 831, 45
D'Aí, A., Di Salvo, T., Ballantyne, D., et al. 2010, A&A, 516, A36
Dauser, T., Wilms, J., Reynolds, C. S., & Brenneman, L. W. 2010, MNRAS, 409, 1534
Degenaar, N., Miller, J. M., Chakrabarty, D., et al. 2015, MNRAS, 451, L85
Degenaar, N., Miller, J. M., Harrison, F. A., et al. 2014, ApJL, 796, L9
Degenaar, N., Altamirano, D., Parker, M., et al. 2016, MNRAS, 461, 4049
Demorest, P. B., Pennucci, T., Ransom, S. M., Roberts, M. S. E., & Hessels, J. W. T. 2010, Natur, 467, 1081
Deutsch, E. W., Margon, B., Anderson, S. F., Wachter, S., & Goss, W. M. 1999, ApJ, 524, 406
Di Salvo, T., Stella, L., Robba, N. R., et al. 2000, ApJL, 544, L119
Di Salvo, T., D'Ai, A., Iaria, R., et al. 2009, MNRAS, 398, 2022
Di Salvo, T., Iaria, R., Matranga, M., et al. 2015, MNRAS, 449, 2794
Dickey, J. M., & Lockman, F. J. 1990, ARA&A, 28, 215
Done, C., Gierliński, M., & Kubota, A. 2007, A&ARv, 15, 1
Egron, E., Di Salvo, T., Motta, S., et al. 2013, A&A, 550, A5
Fabian, A. C., Rees, M. J., Stella, L., & White, N. E. 1989, MNRAS, 238, 729
Frank, J., King, A. R., & Lasota, J.-P. 1987, A&A, 178, 137
Freire, P. C. C., Bassa, C. G., Wex, N., et al. 2011, MNRAS, 412, 2763
Galloway, D. K., Muno, M. P., Hartman, J. M., Psaltis, D., & Chakrabarty, D. 2008, ApJS, 179, 360
García, J. A., Fabian, A. C., Kallman, T. R., et al. 2016, MNRAS, 462, 751
Garcıa, J., Dauser, T., Lohfink, A., et al. 2014, ApJ, 782, 76
Gierliński, M., & Done, C. 2002, MNRAS, 337, 1373
Gilfanov, M., Revnivtsev, M., & Molkov, S. 2003, A&A, 410, 217
González Martínez-País, I., Shahbaz, T., & Casares Velázquez, J. 2014, Accretion Processes in Astrophysics (Cambridge: Cambridge Univ. Press)
Harrison, F. A., Craig, W. W., Christensen, F. E., et al. 2013, ApJ, 770, 103
Hasinger, G., & van der Klis, M. 1989, A&A, 225, 79
Horowitz, C. J., & Piekarewicz, J. 2001, PhRvL, 86, 5647
Jacoby, B. A., Hotan, A., Bailes, M., Ord, S., & Kulkarni, S. R. 2005, ApJL, 629, L113
King, A. L., Tomsick, J. A., Miller, J. M., et al. 2016, ApJL, 819, L29
Kiziltan, B., Kottas, A., De Yoreo, M., & Thorsett, S. E. 2013, ApJ, 778, 66
Kuulkers, E., den Hartog, P. R., in't Zand, J. J. M., et al. 2003, A&A, 399, 663
Langmeier, A., Sztajno, M., Hasinger, G., Truemper, J., & Gottwald, M. 1987, ApJ, 323, 288
Lattimer, J. M. 2011, Ap&SS, 336, 67
Lattimer, J. M., & Prakash, M. 2001, ApJ, 550, 426
Lattimer, J. M., & Prakash, M. 2016, PhR, 621, 127
Lin, D., Remillard, R. A., & Homan, J. 2007, ApJ, 667, 1073
London, R. A., Taam, R. E., & Howard, W. M. 1986, ApJ, 306, 170
Long, M., Romanova, M. M., & Lovelace, R. V. E. 2005, ApJ, 634, 1214
Ludlam, R. M., Miller, J. M., Cackett, E. M., et al. 2016, ApJ, 824, 37
Lyu, M., Méndez, M., Sanna, A., et al. 2014, MNRAS, 440, 1165
Merloni, A., Fabian, A. C., & Ross, R. R. 2000, MNRAS, 313, 193
Miller, J. M. 2007, ARA&A, 45, 441
Miller, J. M., Maitra, D., Cackett, E. M., Bhattacharyya, S., & Strohmayer, T. E. 2011, ApJL, 731, L7
Miller, J. M., Fabian, A. C., Wijnands, R., et al. 2002, ApJL, 570, L69
Miller, J. M., D'Ai, A., Bautz, M. W., et al. 2010, ApJ, 724, 1441
Miller, J. M., Parker, M. L., Fuerst, F., et al. 2013, ApJL, 779, L2
Miller, M. C., Lamb, F. K., & Psaltis, D. 1998, ApJ, 508, 791
Mitsuda, K., Inoue, H., Koyama, K., et al. 1984, PASJ, 36, 741
Ng, C., Díaz Trigo, M., Cadolle Bel, M., & Migliari, S. 2010, A&A, 522, A96
Pandel, D., Kaaret, P., & Corbel, S. 2008, ApJ, 688, 1288
Papitto, A., D'Ai, A., di Salvo, T., et al. 2008, ATel, 1846, 1
Papitto, A., Di Salvo, T., D'Aì, A., et al. 2009, A&A, 493, L39
Papitto, A., D'Ai, A., Di Salvo, T., et al. 2013, MNRAS, 429, 3411
Pedersen, H., Lub, J., Inoue, H., et al. 1982, ApJ, 263, 325
Pintore, F., Sanna, A., Di Salvo, T., et al. 2016, MNRAS, 457, 2988
Piraino, S., Santangelo, A., di Salvo, T., et al. 2007, A&A, 471, L17
Popham, R., & Sunyaev, R. 2001, ApJ, 547, 355
Reis, R. C., Fabian, A. C., Ross, R. R., et al. 2008, MNRAS, 387, 1489
Reis, R. C., Fabian, A. C., Ross, R. R., & Miller, J. M. 2009a, MNRAS, 395, 1257
Reis, R. C., Fabian, A. C., & Young, A. J. 2009b, MNRAS, 399, L1
Reynolds, C. S., & Fabian, A. C. 2008, ApJ, 675, 1048
Ross, R. R., & Fabian, A. C. 1993, MNRAS, 261, 74
Ross, R. R., & Fabian, A. C. 2005, MNRAS, 358, 211
Sanna, A., Hiemstra, B., Méndez, M., et al. 2013, MNRAS, 432, 1144
Sanna, A., Méndez, M., Altamirano, D., et al. 2014, MNRAS, 440, 3275
Shih, I. C., Bird, A. J., Charles, P. A., Cornelisse, R., & Tiramani, D. 2005, MNRAS, 361, 602
Shimura, T., & Takahara, F. 1995, ApJ, 445, 780
Sibgatullin, N. R., & Sunyaev, R. A. 1998, AstL, 24, 774
Sibgatullin, N. R., & Sunyaev, R. A. 2000, AstL, 26, 699
Sleator, C. C., Tomsick, J. A., King, A. L., et al. 2016, ApJ, 827, 134
Strohmayer, T. E., & Markwardt, C. B. 2002, ApJ, 577, 337
Tarenghi, M., & Reina, C. 1972, NPhS, 240, 53
van Paradijs, J., van der Klis, M., van Amerongen, S., et al. 1990, A&A, 234, 181
Verner, D. A., Ferland, G. J., Korista, K. T., & Yakovlev, D. G. 1996, ApJ, 465, 487
Wijnands, R., Homan, J., van der Klis, M., et al. 1997, ApJL, 490, L157
Wilms, J., Allen, A., & McCray, R. 2000, ApJ, 542, 914
Zhang, W., Lapidus, I., Swank, J. H., White, N. E., & Titarchuk, L. 1997, IAU Circ., 6541